ACS APPLIED MATERIALS & INTERFACES

Research Article

Cite This: ACS Appl. Mater. Interfaces 2018, 10, 14914−14921

www.acsami.org

Strain-Driven Nanoscale Phase Competition near the Antipolar−Nonpolar Phase Boundary in $Bi_{0.7}La_{0.3}FeO_3$ Thin Films

Liv R. Dedon,[†,#] Zuhuang Chen,[†,§,#] Ran Gao,[†] Yajun Qi,[†,∥] Elke Arenholz,[⊥] and Lane W. Martin*[,†,‡]

[†]Department of Materials Science and Engineering, University of California, Berkeley, Berkeley, California 94720, United States

[‡]Materials Sciences Division, Lawrence Berkeley National Laboratory, Berkeley, California 94720, United States

[§]School of Materials Science and Engineering, Harbin Institute of Technology, Shenzhen 518055, P. R. China

[∥]Department of Materials Science and Engineering, Hubei University, Wuhan 430062, P. R. China

[⊥]Advanced Light Source, Lawrence Berkeley National Laboratory, Berkeley, California 94720, United States

Supporting Information

ABSTRACT: Complex-oxide materials tuned to be near phase boundaries via chemistry/composition, temperature, pressure, etc. are known to exhibit large susceptibilities. Here, we observe a strain-driven nanoscale phase competition in epitaxially constrained $Bi_{0.7}La_{0.3}FeO_3$ thin films near the antipolar−nonpolar phase boundary and explore the evolution of the structural, dielectric, (anti)ferroelectric, and magnetic properties with strain. We find that compressive and tensile strains can stabilize an antipolar $PbZrO_3$-like *Pbam* phase and a nonpolar *Pnma* orthorhombic phase, respectively. Heterostructures grown with little to no strain exhibit a self-assembled nanoscale mixture of the two orthorhombic phases, wherein the relative fraction of each phase can be modified with film thickness. Subsequent investigation of the dielectric and (anti)ferroelectric properties reveals an electric-field-driven phase transformation from the nonpolar phase to the antipolar phase. X-ray linear dichroism reveals that the antiferromagnetic-spin axes can be effectively modified by the strain-induced phase transition. This evolution of antiferromagnetic-spin axes can be leveraged in exchange coupling between the antiferromagnetic $Bi_{0.7}La_{0.3}FeO_3$ and a ferromagnetic $Co_{0.9}Fe_{0.1}$ layer to tune the ferromagnetic easy axis of the $Co_{0.9}Fe_{0.1}$. These results demonstrate that besides chemical alloying, epitaxial strain is an alternative and effective way to modify subtle phase relations and tune physical properties in rare earth-alloyed $BiFeO_3$. Furthermore, the observation of antiferroelectric-antiferromagnetic properties in the *Pbam* $Bi_{0.7}La_{0.3}FeO_3$ phase could be of significant scientific interest and great potential in magnetoelectric devices because of its dual antiferroic nature.

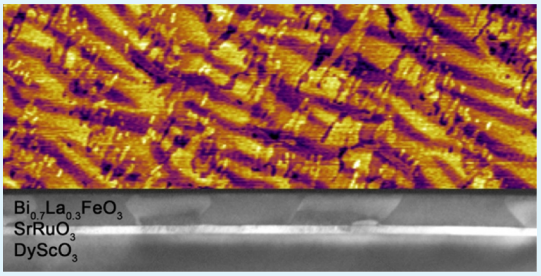

KEYWORDS: *$BiFeO_3$, $Bi_{1-x}La_xFeO_3$, antipolar, phase competition, thin films*

INTRODUCTION

By perching a ferroic material near a phase boundary, it is possible to produce large susceptibilities under application of small external stimuli (e.g., thermal, electric field, magnetic field, etc.).[1−4] For instance, giant dielectric/piezoelectric responses are obtained in ferroelectrics near morphotropic phase boundaries (MPBs).[1] The majority of work on MPB systems has focused on polar−polar boundaries, and there is little work on other systems, such as polar−antipolar and antipolar−nonpolar boundaries. However, as we expand the realm of material systems that we study, more exotic structural boundaries are being found. For example, the multiferroic $BiFeO_3$ is one of the most widely studied ferroic materials in recent years because of its strong room-temperature magnetoelectric coupling between the ferroelectric and antiferromagnetic ordering, which makes it a promising candidate for low-power nanoelectric and spintronic devices.[5−9] Despite exceptional interest and study, the use of $BiFeO_3$ continues to be limited by its high electrical leakage current. The relatively small band gap (~2.7 eV), partially occupied *d* orbitals, and propensity to form point defects that can dope the lattice with charge all contribute to the undesirable leakage.[5,10,11] In turn, there has been research on doping/alloying $BiFeO_3$ to mitigate electronic leakage/conduction, thus enhance the ferroelectric properties, and also as a potential pathway, to improve other properties, including lowering coercivity and increasing piezoelectric response and magnetoelectric coupling.[12] For example, *A*-site alloying with rare earth elements (e.g., Sm, Dy, etc.) has been shown to significantly reduce electronic conduction and to improve the piezoelectric response by emulating MPB-like behavior.[13−15]

In this regard, considerable attention has been devoted to $Bi_{1-x}La_xFeO_3$ solid solutions.[1] This is mainly because La^{3+} and Bi^{3+} have nearly the same ionic radii, which enables perturbation of the ferroelectric order without greatly impacting the magnetic *B* site. Until recently, however, the nature, and

Received: February 12, 2018
Accepted: April 11, 2018
Published: April 11, 2018

DOI: 10.1021/acsami.8b02597
ACS Appl. Mater. Interfaces 2018, 10, 14914−14921

even the exact number, of structural phase transitions as a function of lanthanum content is still an open question.[13] This is mainly because most studies have focused on relatively low fractions of lanthanum addition ($x \lesssim 0.2$) in hopes of maintaining ferroelectricity while lowering the leakage and coercivity.[16,17] For $x \lesssim 0.2$, bulk $Bi_{1-x}La_xFeO_3$ maintains the parent *R*3*c* symmetry and exhibits improved ferroelectric properties.[17] As the lanthanum content increases, things get more interesting as there is a reported polar-to-nonpolar phase transition.[17−26] As noted, there remains disagreement over the exact nature of this phase progression from the ferroelectric *R*3*c* to the paraelectric *Pnma* end members.[13] For instance, first-principles calculations have predicted a direct transition from the rhombohedral *R*3*c* to the orthorhombic *Pnma* phase akin to a MPB-like transition with several quasi-energy-degenerate phases occurring at $x \approx 0.3$.[21,22] Others have reported the existence of intermediate orthorhombic phases (i.e., an antipolar *Pbam* or an incommensurate nonpolar *Imma* phase) between the *R*3*c* and *Pnma* phases.[19,23,24,26−33] Despite these reports, the nature of the orthorhombic phases near the so-called MPB-like transition and their strain and field dependence are still a matter of discussion.

Here, we explore how epitaxial strain impacts the structure, dielectric, (anti)ferroelectric, and magnetic properties near this so-called MPB-like transition in $Bi_{0.7}La_{0.3}FeO_3$ thin films. Epitaxial $Bi_{0.7}La_{0.3}FeO_3$ films are grown on a range of substrates producing epitaxial strains that range from −0.7% to +1.1%. It is found that compressive strain stabilizes a single-phase, antipolar $PbZrO_3$-type *Pbam* orthorhombic phase, that tensile strain stabilizes a single-phase, nonpolar *Pnma* orthorhombic phase, and that growth with essentially zero strain results in a self-assembled nanoscale mixture of the two orthorhombic phases, wherein the relative fraction of each phase can be modified with film thickness. Subsequent investigation of the dielectric and (anti)ferroelectric properties reveals an electric-field-driven irreversible phase transformation from the nonpolar to the antipolar phase. X-ray linear dichroism and exchange coupling studies further reveal that the antiferromagnetic-spin orientation in the $Bi_{0.7}La_{0.3}FeO_3$ thin films and subsequently the magnetic anisotropy of a coupled ferromagnetic layer can be effectively tuned by the strain-induced phase transition.

RESULTS AND DISCUSSION

$Bi_{0.7}La_{0.3}FeO_3$ (~90 nm)/$SrRuO_3$ (20 nm) bilayers were grown on $SrTiO_3$(001), $DyScO_3(110)_O$, and $GdScO_3(110)_O$ single-crystal substrates using pulsed-laser deposition (Materials and Methods). Note that we will use cubic or pseudocubic indices throughout this paper unless otherwise specified, and the subscript "O" denotes orthorhombic indices. Following growth, wide-angle θ−2θ scan X-ray diffraction studies (Supporting Information, Figure S1) reveal that all $Bi_{0.7}La_{0.3}FeO_3$ heterostructures are fully epitaxial and 00*l*-oriented. Closer examination of the 002-diffraction condition of the $Bi_{0.7}La_{0.3}FeO_3$ films reveals marked shifts in peak position, consistent with varying degrees of lattice parameter mismatch between the $Bi_{0.7}La_{0.3}FeO_3$ film and the underlying substrate (Figure 1a). Consistent with the observed Laue oscillations and small full width at half-maximum in the θ−2θ scans, all heterostructures (Figure 1b−g) show atomically smooth surface morphologies in atomic force microscopy (AFM). In the bulk, $Bi_{0.7}La_{0.3}FeO_3$ exhibits an orthorhombic structure at room temperature with lattice parameters of a = 5.572 Å, b = 5.554 Å, and c = 7.864 Å.[19] Films grown on $SrRuO_3$-buffered

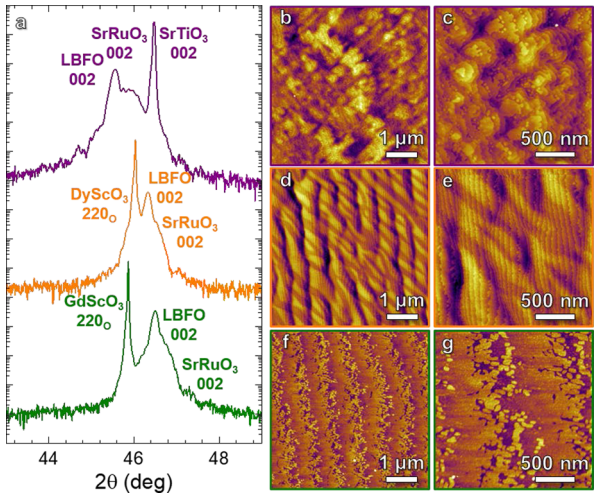

Figure 1. (a) θ−2θ X-ray diffraction patterns about the 002-diffraction conditions of the $Bi_{0.7}La_{0.3}FeO_3$ film and $SrRuO_3$ bottom electrode and 002-diffraction condition of $SrTiO_3$ and 220-diffraction conditions of the $GdScO_3$, $DyScO_3$ substrates. AFM studies of films grown on (b,c) $SrTiO_3$, (d,e) $DyScO_3$, and (f,g) $GdScO_3$ substrates revealing the appearance of mixed-phase structures for films grown on $DyScO_3$ substrates.

$SrTiO_3$ (−0.7% lattice mismatch, Figure 1b,c) and $GdScO_3$ (+1.1% lattice mismatch, Figure 1f,g) substrates show a uniform height contrast (with the exception of surface terraces from the substrate). In contrast, heterostructures grown on $SrRuO_3$-buffered $DyScO_3$ (0.3% lattice mismatch, Figure 1d,e) exhibit intricate nanoscale stripes in surface height with 3.4 ± 0.3 Å of height difference (corresponding to a ~0.4% change in the out-of-plane thickness) between the high (light) and low (dark) regions. The relative fraction of high and low stripes shifts as the film thickness is increased, with the fraction of high regions growing as the film thickness is increased (Supporting Information, Figure S2). This stripe morphology and its thickness-dependent evolution are reminiscent of a strain-mediated, mixed-phase structure with enhanced electromechanical response in highly strained $BiFeO_3$ films[34] and suggest that there could be strain-induced phase coexistence in heterostructures grown on $DyScO_3$.

Reciprocal space mapping (RSM) studies probed the strain state and the lattice parameters of the films. RSM studies about the 013-diffraction condition of the film and 013-diffraction condition of $SrTiO_3$ and 420_O-diffraction condition of the $DyScO_3$ and $GdScO_3$ substrates (Figure 2a−c) reveal two important points: (1) all heterostructures are essentially coherently strained to the respective substrates and (2) heterostructures grown on $SrTiO_3$ and $GdScO_3$ substrates exhibit only one phase (as illustrated by the single diffraction peak), whereas those grown on $DyScO_3$ appear to consist of two distinct phases (as indicated by the presence of two distinct diffraction peaks). We note that, in the latter case, elastic domains or twins could potentially give rise to multiple diffraction peaks. Below, we will describe additional studies that confirm that this diffraction pattern arises from two phases. The data together with additional RSM studies at different diffraction conditions (Supporting Information, Figures S3−S5) allow for the extraction of the unit-cell parameters for the various phases, which are thus summarized (Figure 2d); this includes two distinct phases for the films grown on $SrTiO_3$ and $GdScO_3$ and a mixture of phases on $DyScO_3$.

DOI: 10.1021/acsami.8b02597
ACS Appl. Mater. Interfaces 2018, 10, 14914−14921

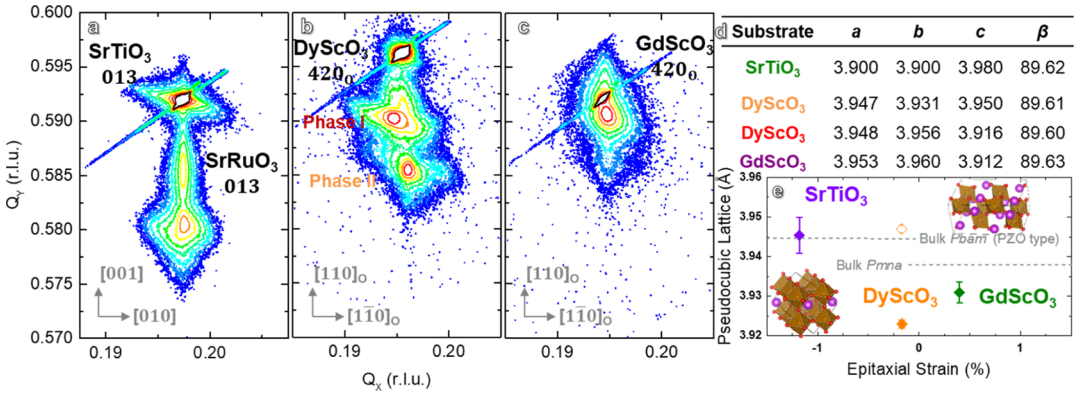

Figure 2. RSM studies about the (a) 013-diffraction condition of the $SrTiO_3$ substrate and the 420_O-diffraction conditions of the (b) $DyScO_3$ and (c) $GdScO_3$ substrates showing only a single peak for the $SrTiO_3$ and $GdScO_3$ heterostructures (confirming the presence of a single phase) but two clear diffraction peaks for films grown on $DyScO_3$ substrates. (d) Experimentally extracted lattice parameters consistent with coexistence of the phases observed on $SrTiO_3$ and $GdScO_3$. The extracted lattice parameters agree well with (e) reported lattice parameters for both *Pnma* and *Pbam* phases.

To further understand the nature of the crystal structures, various RSM studies were conducted to investigate quarter-order diffraction peaks (as their presence indicates a structure which is compatible with antipolar order).[12,13] Focusing first on the compressively strained films grown on $SrTiO_3$ substrates, RSM studies (Supporting Information, Figure S3c) reveal the presence of such quarter-order diffraction peaks. These results, combined with the extracted lattice parameters (Figure 2d), are consistent with reports in the literature of a $PbZrO_3$-type *Pbam* phase.[13,23,24,32,33] Shifting our focus to the tensile-strained films grown on $GdScO_3$ substrates, no evidence of quarter-order diffraction peaks was observed (Supporting Information, Figure S4d). This result combined with the extracted lattice parameters (Figure 2d) indicates a second orthorhombic phase that agrees closely with both the incommensurate $Imma(00\gamma)s00$ superstructure and *Pnma* phases that have been previously observed.[19,30,35] The *Pnma* phase is the most widely reported nonpolar phase in the rare earth-alloyed $BiFeO_3$ system,[13,19,35] but there has been some disagreement over whether the $Imma(00\gamma)s00$ superstructure phase is an intermediate nonpolar phase. To further complicate phase identification, the $Imma(00\gamma)s00$ superstructure phase was initially incorrectly indexed as a conventional *Imma* phase with secondary parasitic phases.[29,30] This oversimplified assignment was subsequently amended based on the persistence of the superstructure peaks with varied synthesis conditions.[19,30] A second $Pn2_1a(00\gamma)s00$ superstructure has also been reported in bulk $Bi_{0.7}La_{0.3}FeO_3$ and has been differentiated from the $Imma(00\gamma)s00$ superstructure only by minute changes in the superstructure diffraction peaks.[35,36] We can rule out the presence of either of the two superstructured phases because satellite peaks are not observed in the X-ray diffraction patterns (Supporting Information, Figure S1) nor in transmission electron microscopy (TEM) selected area electron diffraction (SAED, discussed later). The lack of both quarter-order and superstructure satellite diffraction peaks confirms that the tensile-strained heterostructures grown on $GdScO_3$ are a single nonpolar *Pnma* phase.

Finally, we focus our attention on films grown on $DyScO_3$ substrates which show evidence of seeming nanoscale phase coexistence. Synchrotron-based diffraction studies (Materials and Methods) reveal clear quarter-order peaks (Supporting Information, Figure S5b), indicating the presence of the compressively strained *Pbam* phase as observed in the heterostructures grown on $SrTiO_3$. The uneven intensity distribution between the observed quarter-order peaks suggests that there is a preferred orientation, which is likely the result of the orthorhombic nature of the $DyScO_3$ substrate.[37] The lattice parameters of the second phase observed in the heterostructures grown on $DyScO_3$ agree with an epitaxially strained *Pnma* phase, as observed in heterostructures grown on $GdScO_3$ (Figure 2e). This observation is further supported by cross-sectional TEM imaging of heterostructures grown on $DyScO_3$ (Figure 3a), which reveals bands of varying light and dark contrast on the same length scale as the stripes observed with AFM (Figure 1e). SAED patterns (Figure 3b,c) of the two different regions show clear differences in structure, confirming the coexistence of two phases in heterostructures grown on $DyScO_3$ as observed from the RSM studies (Figure 2a–c). The first selected region within a darker contrast stripe has a SAED pattern (Figure 3b) consistent with the *Pnma* phase. The lack

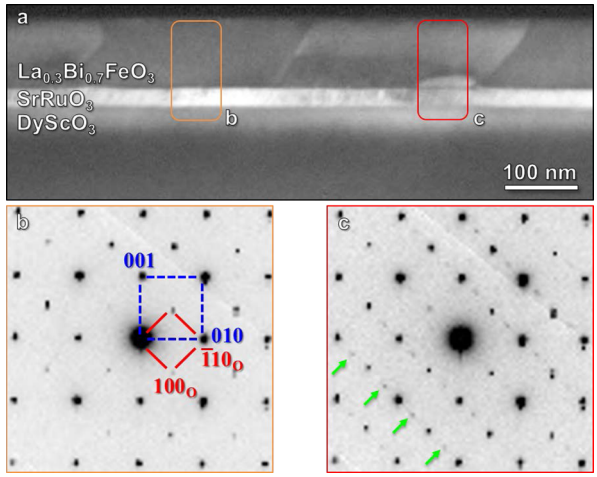

Figure 3. (a) Transmission electron micrograph of the $Bi_{0.7}La_{0.3}FeO_3$ heterostructure on $SrRuO_3$-buffered $DyScO_3$, viewed along the substrate $[001]_O$, revealing the presence of phase coexistence. SAED patterns taken of the marked regions for the (b) *Pnma* and (c) *Pbam* phases. The superlattice ordering corresponding to the highlighted 1/4 $(0\bar{1}1)$ reflections (as marked by the arrows in c) indicates the antipolar structure with a space group of *Pbam*.

DOI: 10.1021/acsami.8b02597
ACS Appl. Mater. Interfaces 2018, 10, 14914–14921

of additional reflections in the diffraction pattern supports this conclusion as both superstructured phases would have clear superlattice spots. The second region, within a lighter contrast stripe, has a SAED pattern (Figure 3c), which is consistent with the RSM studies, where superlattice spots corresponding to the highlighted 1/4 $(0\bar{1}1)$ reflections (as marked by the arrows, Figure 3c) indicate that the region exhibits an antipolar structure with a space group of *Pbam*. Thus, it appears that at small strains, as is the case for films grown on $DyScO_3$ substrates, an intimate mixture of the two nanoscale phases is observed. This demonstrated ability to control phase stability using epitaxial strain in $Bi_{0.7}La_{0.3}FeO_3$ has not been previously reported.

Because of the difference in structure between the compressively stabilized *Pbam* and tensile-stabilized *Pnma* phases, it is expected that heterostructures grown on $SrTiO_3$ and $GdScO_3$ will show antipolar and nonpolar electrical responses, respectively. The coexistence of both antipolar and nonpolar phases in heterostructures grown on $DyScO_3$, however, begs the question as to whether one can electrically control the phases and if there is potential for unexpected electrical properties. Polarization−electric field hysteresis loops were measured at room temperature (Materials and Methods; Supporting Information Figure S6) but were inconclusive because of leakage currents obscuring the true loop shape. The issue is that even though lanthanum addition is known to increase the resistance of $BiFeO_3$, the amount added herein also drives the electric fields (voltage) required to switch the material to such high levels that considerable leakage is observed. As such, additional electrical measurements were performed at 200 K to minimize the leakage behavior under the large fields required to saturate the response. Heterostructures grown on $SrTiO_3$ (Figure 4a) and $DyScO_3$ (Figure 4b) substrates exhibit pinched hysteresis loops regardless of the magnitude of the applied fields. This behavior is not unexpected considering the presence of the antipolar (and potentially antiferroelectric) *Pbam* phase in both cases. For heterostructures grown on $GdScO_3$, however, the presence of the nonpolar *Pnma* phase results in a linear response at subcoercive fields but abruptly transitions to show the same pinched hysteresis loops above a threshold applied field (Figure 4c). These pinched hysteresis loops persist as the voltage is decreased below the coercive field and does not appear to relax back to show the initially observed linear response after up to 2 h in zero bias, suggesting an irreversible phase transition from the nonpolar to the antipolar (and potentially antiferroelectric) phase. Such pinched hysteresis loops are observed in all heterostructure variants across a range of measurement frequencies (Supporting Information Figure S7).

To further verify the potential field-induced phase transition from the nonpolar *Pnma* to the antipolar *Pbam* phase, poling experiments were done using piezoresponse force microscopy on heterostructures grown on $DyScO_3$ to track changes in surface morphology with applied bias (Figure 4d−f). The obtained height images demonstrate persistent transformation of the smaller out-of-plane lattice parameter minority *Pnma* phase (dark stripes) to the larger out-of-plane lattice parameter majority *Pbam* phase (lighter background) with the application of both positive and negative bias. A 11% (2%) and a 16% (10%) decrease in the fraction of low stripes from the as-grown state are observed after the application of −10 V (+10 V) (Figure 4e) and −20 V (+20 V) (Figure 4f), respectively. It is important to note that height images (Figure 4d−f) do not

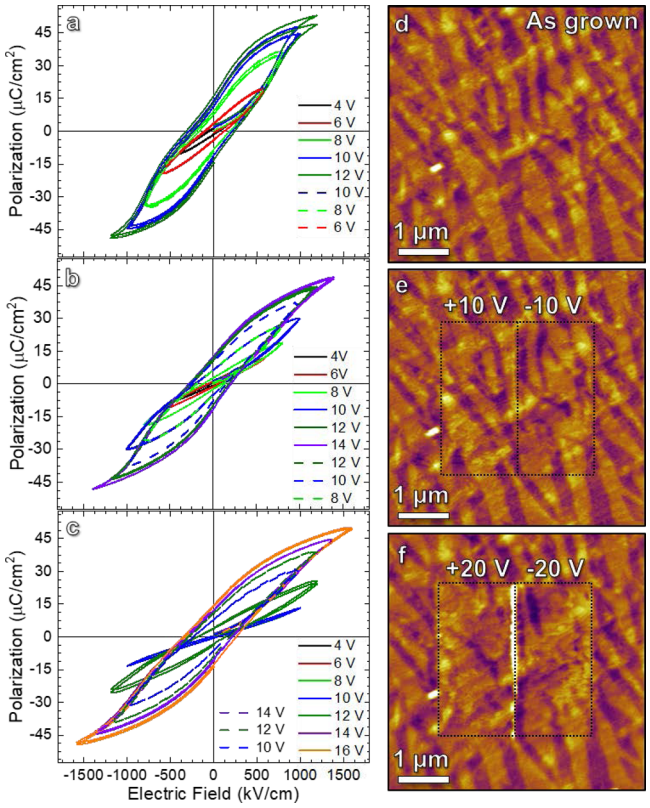

Figure 4. Polarization−electric field hysteresis loops for $La_{0.3}Bi_{0.7}FeO_3$ heterostructures on $SrRuO_3$-buffered (a) $SrTiO_3$, (b) $DyScO_3$, and (c) $GdScO_3$ measured at 200 K. Films grown on $SrTiO_3$ and $DyScO_3$ substrates show persistent antiferroelectric-like behavior from subsaturation through fully saturated loops. Films grown on $GdScO_3$ substrates exhibit linear dielectric response at low applied fields and transition to an antiferroelectric-like loop above a threshold field. This voltage-induced phase transformation is observed in films grown on $DyScO_3$ as the surface morphology changes from the (d) as-grown state with poling with (e) ±10 V and (f) ±20 V in the areas marked with the square.

convey any information about the piezoresponse of the $Bi_{0.7}La_{0.3}FeO_3$ heterostructure. The piezoresponse data obtained during the measurements are consistent with the antipolar and nonpolar nature of the constituent phases. The only contrast in the piezoresponse data was observed in the poled areas and quickly dissipated after poling, which is consistent with transient charging due to the large applied voltage used in the poling study. On the basis of the significant change in relative fractions of light and dark regions after poling, it is concluded that a voltage-induced phase transformation takes place, driving the nonpolar *Pnma* phase (dark regions) to the antipolar *Pbam* phase (light stripes). To the best of our knowledge, this is the first experimental observation of an electric-field-driven nonpolar-to-antipolar phase transition in $Bi_{1-x}La_xFeO_3$. We note that although electric-field-driven nonpolar orthorhombic to polar rhombohedral phase transitions for other rare earth-doped $BiFeO_3$ systems with higher chemical pressure (e.g., Dy and Sm) have been reported,[14] such a field-driven transition has been dismissed in the case of low chemical pressure alloying with La because of the lack of nanoscale phase coexistence and the lack of observed d_{33} enhancement under applied bias.[12,20,24,38] This said, first-principles calculations have predicted several low-energy metastable orthorhombic phases in $Bi_{0.7}La_{0.3}FeO_3$ and further

DOI: 10.1021/acsami.8b02597
ACS Appl. Mater. Interfaces 2018, 10, 14914−14921

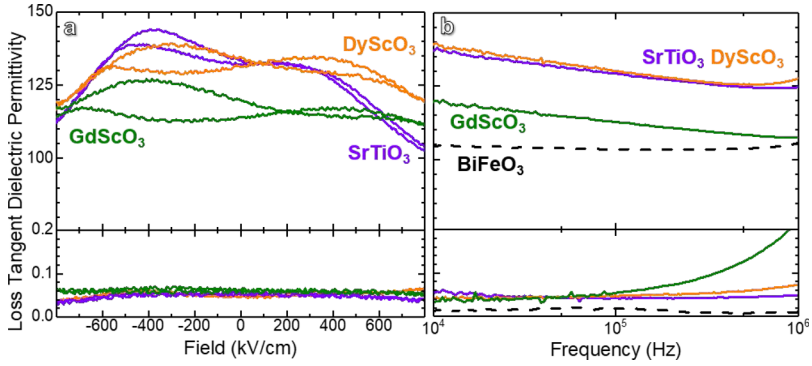

Figure 5. (a) Dielectric permittivity (top) and loss tangent (bottom) vs applied field for all three heterostructures showing an antiferroelectric-like double-bump shape consistent with the antiferroelectric-like hysteresis loops. (b) Dielectric permittivity vs frequency at 200 K for all heterostructure variants compared with a $BiFeO_3$ heterostructure of comparable thickness.

suggest that an electric field might be used to induce phase transformations between those nearly-energy-degenerate phases.[22] Such predictions are consistent with our observations.

The observed pinched hysteresis loops and the potential for antiferroelectric-like behavior are further supported by capacitance/dielectric permittivity−voltage measurements (Figure 5a). The heterostructures clearly do not show the prototypical ferroelectric shape and instead are more reminiscent of antiferroelectric-like behavior. It is important to note that the heterostructures grown on $GdScO_3$ are expected to show antiferroelectric-like behavior as the measurement started from negative bias, poling the sample into the antipolar (and potentially antiferroelectric-like) state for the remainder of the measurement. Heterostructures grown on $SrTiO_3$ and $DyScO_3$ are expected to show antipolar (and potentially antiferroelectric-like) behavior regardless of starting voltage because of their as-grown *Pbam* phase that is further reinforced by the applied bias. This is all consistent with what is expected for the antipolar *Pbam* phase.[39] The dielectric constant of the $Bi_{0.7}La_{0.3}FeO_3$ heterostructures (~140 for heterostructures grown on both $SrTiO_3$ and $DyScO_3$ and ~120 for the heterostructure grown on $GdScO_3$; 10 kHz, Figure 5b) is higher than that of a similarly grown $BiFeO_3$ heterostructure (~105, which is consistent with previous reports[20]).

Thus, having shown that epitaxial strain can effectively tune the structural and electric properties of $Bi_{1-x}La_xFeO_3$, we now concentrate on how the strain affects the magnetic properties. Bulk $BiFeO_3$ exhibits G-type antiferromagnetism with a superimposed long-wavelength cycloidal modulation and a Néel temperature $T_N \approx 643$ K, whereas bulk $LaFeO_3$ is a simple G-type antiferromagnet with $T_N \approx 750$ K. It is reported that epitaxial strain or chemical alloying with rare earth elements can suppress the spin cycloid and drive a transition toward a homogenous weakly ferromagnetic order in $BiFeO_3$. Angle- and polarization-dependent linear X-ray absorption spectroscopy (XAS) measurements were carried out on the $Bi_{0.7}La_{0.3}FeO_3$ films to study the effect of strain on the antiferromagnetic order. The Fe $L_{2,3}$ XAS spectral shape depends on the relative orientation of the polarization vector $\vec{E}$ of the incoming X-rays, the crystallographic axes, and the antiferromagnetic-spin axis L. Representative pairs of absorption spectra [taken in normal incidence with $\vec{E}$ parallel to [100] (orange curves), [010] (blue curves), [110] (red curves), and [1$\bar{1}$0] (green curves)] are provided (Figure 6a−c). These studies demonstrate that strain and the resulting structural change can effectively tune the spin orientation of the films. For $Bi_{0.7}La_{0.3}FeO_3$ heterostructures

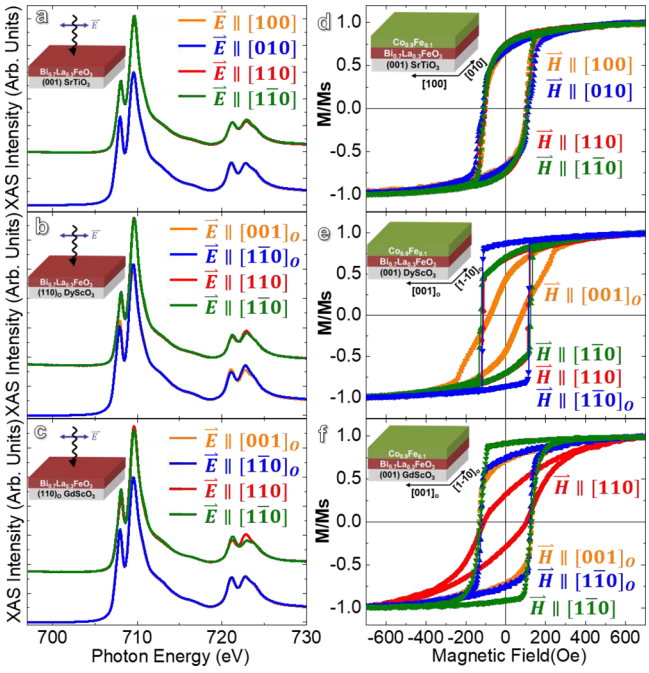

Figure 6. Polarization-dependent XAS measurements at normal incidence for films grown on (a) $SrTiO_3$ (showing no anisotropy, dichroism) (b) $DyScO_3$ (showing clear dichroism with incident light along $[001]_O$), and (c) $GdScO_3$ (showing clear dichroism with incident light along $[1\bar{1}0]$) substrates. MOKE measurements for $Co_{0.9}Fe_{0.1}/Bi_{0.7}La_{0.3}FeO_3$ heterostructures grown on (d) $SrTiO_3$, (e) $DyScO_3$, and (f) $GdScO_3$ substrates showing clear anisotropy when grown on $DyScO_3$ and $GdScO_3$ substrates.

grown on $SrTiO_3$ (Figure 6a), essentially no linear dichroism is revealed in the normal-incidence geometry, indicating that the antiferromagnetic-spin axis is likely along the out-of-plane [001]. For $Bi_{0.7}La_{0.3}FeO_3$ heterostructures grown on $DyScO_3$ (Figure 6b), large dichroism between X-ray with polarization lying along $[001]_O$ and $[1\bar{1}0]_O$ is observed, whereas no dichroism is observed between X-ray with polarization lying along [110] and [1$\bar{1}$0], indicating that the antiferromagnetic-spin axis is likely along the in-plane $[001]_O$. In contrast, for $Bi_{0.7}La_{0.3}FeO_3$ heterostructures grown on $GdScO_3$ (Figure 6c), large dichroism is observed between light with polarization lying along [110] and [1$\bar{1}$0], whereas no dichroism is observed between light with polarization lying along $[001]_O$ and $[1\bar{1}0]_O$, indicating that the antiferromagnetic-spin axis is likely along the

DOI: 10.1021/acsami.8b02597
ACS Appl. Mater. Interfaces 2018, 10, 14914−14921

in-plane [110]. These spectroscopic studies demonstrate that the antiferromagnetic-spin axis of the $Bi_{0.7}La_{0.3}FeO_3$ films is very sensitive to the strain and local structural distortion; therefore, a small change in the amount of strain could drive a significant amount of spin reorientation. This is probably due to a negligibly small magnetic anisotropy energy in Fe^{3+}, as a similar behavior has been observed in $BiFeO_3$ and Fe_2O_3.[40−42]

Exchange coupling of the $Bi_{0.7}La_{0.3}FeO_3$ layers with the ferromagnet $Co_{0.9}Fe_{0.1}$ provides further evidence for the significant effect of the strain-induced phase transition on the magnetic response. Pt (2.5 nm)/$Co_{0.9}Fe_{0.1}$ (2.5 nm) bilayers were grown on the $Bi_{0.7}La_{0.3}FeO_3$ films. Representative magneto-optical Kerr effect (MOKE) hysteresis loops taken from the $Co_{0.9}Fe_{0.1}/Bi_{0.7}La_{0.3}FeO_3$ heterostructures reveal several important points: (1) All heterostructures show an enhancement of the coercive field of $Co_{0.9}Fe_{0.1}$, compared to $Co_{0.9}Fe_{0.1}$ grown on bare substrates (Supporting Information, Figure S8), indicating that a robust exchange coupling is established between the $Bi_{0.7}La_{0.3}FeO_3$ and $Co_{0.9}Fe_{0.1}$. (2) Isotropic response is observed for heterostructures/multilayers grown on $SrTiO_3$ (Figure 6d), whereas clear anisotropy is observed for heterostructures grown on $DyScO_3$ and $GdScO_3$. For heterostructures grown on $DyScO_3$ and $GdScO_3$, the ferromagnetic easy axis is along $[1\bar{1}0]_O$ and $[1\bar{1}0]$, respectively, indicating a perpendicular coupling between the antiferromagnetic-spin axis in $Bi_{0.7}La_{0.3}FeO_3$ and the ferromagnetic spin in the $Co_{0.9}Fe_{0.1}$ layers. (3) The exchange coupling between the antiferromagnetic-spin axis in $Bi_{0.7}La_{0.3}FeO_3$ and the ferromagnetic-spin axis in $Co_{0.9}Fe_{0.1}$ is strong enough to overcome the substrate asymmetry. Without the $Bi_{0.7}La_{0.3}FeO_3$ layer, the easy axis of the $Co_{0.9}Fe_{0.1}$ film is always along $[001]_O$ on the orthorhombic $DyScO_3$ and $GdScO_3$ substrates. In summary, these magnetic studies demonstrate that strain could effectively tune the antiferromagnetic-spin axis and, in turn, the magnetic anisotropy of an exchange-coupled ferromagnet.

CONCLUSIONS

We have demonstrated that epitaxial strain can drive nanoscale phase competition at an antipolar−nonpolar phase boundary in antiferromagnetic $Bi_{0.7}La_{0.3}FeO_3$ thin films and that this coexistence has important implications for material properties. The nonpolar *Pnma* phase, typically observed at higher lanthanum-concentration levels, is stabilized by the tensile strain imposed by the $GdScO_3$ substrate, whereas the compressive strain from the $SrTiO_3$ substrate stabilizes the antipolar $PbZrO_3$-like *Pbam* phase. In the case of small strain, a self-assembled mixture of the two orthorhombic phases is observed. In this mixed-phase system, applied voltage can be used to transform the nonpolar phase to the antipolar phase; a phenomenon not previously observed in the $Bi_{1-x}La_xFeO_3$ system. Subsequent investigation of the magnetic properties reveals a strain-induced rotation of the antiferromagnetic-spin axis. This work provides insights into the complex and subtle nature of phase relations in the rare earth-alloyed $BiFeO_3$ system that could, in turn, allow for enhanced functionality.

MATERIALS AND METHODS

Film Growth. $Bi_{0.7}La_{0.3}FeO_3$ heterostructures were grown via pulsed-laser deposition in an on-axis geometry using a KrF excimer laser (Compex, Coherent) on 20 nm $SrRuO_3/SrTiO_3(001)$, $DyScO_3(110)$, and $GdScO_3(110)$ single-crystal substrates (CrysTec GmbH). The $SrRuO_3$ films, to be used as a bottom electrode for subsequent electrical studies, were grown at a heater temperature of 700 °C, in a dynamic oxygen pressure of 100 mTorr, with a laser energy density of 1.2 J/cm^2, and a laser repetition rate of 15 Hz from a ceramic target of composition $SrRuO_3$. The $BiFeO_3$ films were grown at a heater temperature of 700 °C, in a dynamic oxygen pressure of 100 mTorr, with a laser energy density of 1.1 J/cm^2, and a laser repetition rate of 20 Hz from ceramic targets of composition $Bi_{0.9}La_{0.3}FeO_3$. All substrates were adhered to the heater with Ag paint (Ted Pella, Inc.), and following growth, the heterostructures were cooled to room temperature at a rate of 10 °C/min in 700 Torr of oxygen.

Structural, Chemical, and Physical Property Measurement. Following growth, a variety of techniques were used to probe the structural, electrical, and magnetic properties. Structural studies were performed using high-resolution X-ray diffraction and RSM (PANalytical, X'pert^3 MRD). Synchrotron X-ray RSM studies were conducted at the Advanced Photon Source, Argonne National Laboratory, Sector 33-BM, using the Pilatus 100K detector. Cross-sectional TEM specimens were prepared using the standard procedure consisting of cutting, gluing, mechanical polishing, and ion milling. The ion milling process was performed on a Precision Ion Polishing System (PIPS, model 695, Gatan) with an incident ion angle of 5° and an accelerating voltage of 3 kV using liquid N_2 to cool the stage. TEM investigations were carried out on a JEOL 3010 transmission electron microscope operated at 300 kV. Film morphology was imaged using AFM, with an MFP-3D microscope (Asylum Research). For electrical, dielectric, and ferroelectric studies, symmetric capacitor structures were fabricated by ex situ deposition of 80 nm thick $SrRuO_3$ top electrodes defined using a MgO hard-mask process.[43] Ferroelectric polarization hysteresis loops were measured using a Precision Multiferroic Tester (Radiant Technologies), and dielectric and loss tangent measurements were performed using an E4890 LCR meter (Agilent/Keysight) for frequencies up to 1 MHz. All electrical measurements were performed in a vacuum probe station (TTPX, Lakeshore) with a 336 temperature controller (Lakeshore) at room temperature or at 200 K to minimize leakage behavior. Magnetic hysteresis loop measurements were carried out using the longitudinal MOKE.[44] X-ray spectroscopy measurements were carried out at beamline 4.0.2 of the Advanced Light Source at Lawrence Berkeley National Laboratory. The measurements were performed in total-electron-yield geometry. The XLD measurements were obtained from the difference of horizontal and vertical polarized light absorption spectra. The X-ray beam was incident on the sample at an angle of 90° from the sample surface for normal incidence.

ASSOCIATED CONTENT

Supporting Information

The Supporting Information is available free of charge on the ACS Publications website at DOI: 10.1021/acsami.8b02597.

Experimental growth and characterization methods, additional X-ray diffraction patterns and reciprocal space maps, information on thickness-dependent surface morphology development of mixed-phase films, and additional ferroelectric and magnetic measurement results (PDF)

AUTHOR INFORMATION

Corresponding Author

*E-mail: lwmartin@berkeley.edu.

ORCID

Lane W. Martin: 0000-0003-1889-2513

Author Contributions

#L.R.D. and Z.C. contributed equally to this work.

Notes

The authors declare no competing financial interest.

DOI: 10.1021/acsami.8b02597
ACS Appl. Mater. Interfaces 2018, 10, 14914−14921

■ ACKNOWLEDGMENTS

L.R.D. acknowledges support of the U.S. Department of Energy, Office of Science, Office of Basic Energy Sciences, under award number DE-SC-0012375 for development of the $BiFeO_3$ materials. Z.C. acknowledges support of the U.S. Department of Energy, Office of Science, Office of Basic Energy Sciences, Materials Sciences and Engineering Division, under contract no. DE-AC02-05-CH11231: Materials Project program KC23MP. R.G. acknowledges support of the National Science Foundation under grant OISE-1545907. Y.Q. acknowledges support of the National Science Foundation of China under grant 51472078. L.W.M. acknowledges support from the National Science Foundation under grant DMR-1708615. This research used resources of the Advanced Light Source, which is a DOE Office of Science User Facility under contract no. DE-AC02-05CH11231. Work at the Molecular Foundry (National Center for Electron Microscopy) was supported by the Office of Science, Office of Basic Energy Sciences, of the U.S. Department of Energy under contract no. DE-AC02-05CH11231.

■ REFERENCES

(1) Cox, D. E.; Noheda, B.; Shirane, G.; Uesu, Y.; Fujishiro, K.; Yamada, Y. Universal Phase Diagram for High-Piezoelectric Perovskite Systems. *Appl. Phys. Lett.* **2001**, *79*, 400−402.

(2) Damjanovic, D. A Morphotropic Phase Boundary System Based on Polarization Rotation and Polarization Extension. *Appl. Phys. Lett.* **2010**, *97*, 062906.

(3) Sando, D.; Xu, B.; Bellaiche, L.; Nagarajan, V. A Multiferroic on the Brink: Uncovering the Nuances of Strain-Induced Transitions in $BiFeO_3$. *Appl. Phys. Rev.* **2016**, *3*, 011106.

(4) Jang, B.-K.; Lee, J. H.; Chu, K.; Sharma, P.; Kim, G.-Y.; Ko, K.-T.; Kim, K.-E.; Kim, Y.-J.; Kang, K.; Jang, H.-B.; et al. Electric-Field-Induced Spin Disorder-to-Order Transition near a Multiferroic Triple Phase Point. *Nat. Phys.* **2017**, *13*, 189−196.

(5) Catalan, G.; Scott, J. F. Physics and Applications of Bismuth Ferrite. *Adv. Mater.* **2009**, *21*, 2463−2485.

(6) Martin, L. W.; Schlom, D. G. Advanced Synthesis Techniques and Routes to New Single-Phase Multiferroics. *Curr. Opin. Solid State Mater. Sci.* **2012**, *16*, 199−215.

(7) Lu, C.; Hu, W.; Tian, Y.; Wu, T. Multiferroic Oxide Thin Films and Heterostructures. *Appl. Phys. Rev.* **2015**, *2*, 021304.

(8) Damodaran, A. R.; Agar, J. C.; Pandya, S.; Chen, Z.; Dedon, L.; Xu, R.; Apgar, B.; Saremi, S.; Martin, L. W. New Modalities of Strain-Control of Ferroelectric Thin Films. *J. Phys.: Condens. Matter* **2016**, *28*, 263001.

(9) Fiebig, M.; Lottermoser, T.; Meier, D.; Trassin, M. The Evolution of Multiferroics. *Nat. Rev. Mater.* **2016**, *1*, 16046.

(10) Basu, S. R.; Martin, L. W.; Chu, Y. H.; Gajek, M.; Ramesh, R.; Rai, R. C.; Xu, X.; Musfeldt, J. L. Photoconductivity in $BiFeO_3$ Thin Films. *Appl. Phys. Lett.* **2008**, *92*, 091905.

(11) Ihlefeld, J. F.; Podraza, N. J.; Liu, Z. K.; Rai, R. C.; Xu, X.; Heeg, T.; Chen, Y. B.; Li, J.; Collins, R. W.; Musfeldt, J. L.; et al. Optical Band Gap of $BiFeO_3$ Grown by Molecular-Beam Epitaxy. *Appl. Phys. Lett.* **2008**, *92*, 142908.

(12) Yang, C.-H.; Kan, D.; Takeuchi, I.; Nagarajan, V.; Seidel, J. Doping $BiFeO_3$: Approaches and Enhanced Functionality. *Phys. Chem. Chem. Phys.* **2012**, *14*, 15953.

(13) Arnold, D. C. Composition-Driven Structural Phase Transitions in Rare-Earth-Doped $BiFeO_3$ Ceramics: A Review. *IEEE Trans. Ultrason. Ferroelectr. Freq. Control* **2015**, *62*, 62−82.

(14) Kan, D.; Pálová, L.; Anbusathaiah, V.; Cheng, C. J.; Fujino, S.; Nagarajan, V.; Rabe, K. M.; Takeuchi, I. Universal Behavior and Electric-Field-Lnduced Structural Transition in Rare-Earth-Substituted $BiFeO_3$. *Adv. Funct. Mater.* **2010**, *20*, 1108−1115.

(15) Fujino, S.; Murakami, M.; Anbusathaiah, V.; Lim, S.-H.; Nagarajan, V.; Fennie, C. J.; Wuttig, M.; Salamanca-Riba, L.; Takeuchi, I. Combinatorial Discovery of a Lead-Free Morphotropic Phase Boundary in a Thin-Film Piezoelectric Perovskite. *Appl. Phys. Lett.* **2008**, *92*, 202904.

(16) Singh, S. K.; Maruyama, K.; Ishiwara, H. The Influence of La-Substitution on the Micro-Structure and Ferroelectric Properties of Chemical-Solution-Deposited $BiFeO_3$ Thin Films. *J. Phys. D: Appl. Phys.* **2007**, *40*, 2705−2709.

(17) Chu, Y. H.; Zhan, Q.; Yang, C.-H.; Cruz, M. P.; Martin, L. W.; Zhao, T.; Yu, P.; Ramesh, R.; Joseph, P. T.; Lin, I. N.; et al. Low Voltage Performance of Epitaxial $BiFeO_3$ Films on Si Substrates through Lanthanum Substitution. *Appl. Phys. Lett.* **2008**, *92*, 102909.

(18) Zhang, S.-T.; Zhang, Y.; Lu, M.-H.; Du, C.-L.; Chen, Y.-F.; Liu, Z.-G.; Zhu, Y.-Y.; Ming, N.-B.; Pan, X. Q. Substitution-Induced Phase Transition and Enhanced Multiferroic Properties of Bi1-XLaxFeO3 Ceramics. *Appl. Phys. Lett.* **2006**, *88*, 162901.

(19) Rusakov, D. A.; Abakumov, A. M.; Yamaura, K.; Belik, A. A.; Van Tendeloo, G.; Takayama-Muromachi, E. Structural Evolution of the $BiFeO_3$−$LaFeO_3$ System. *Chem. Mater.* **2011**, *23*, 285−292.

(20) Cheng, C.-J.; Kan, D.; Anbusathaiah, V.; Takeuchi, I.; Nagarajan, V. Microstructure-Electromechanical Property Correlations in Rare-Earth-Substituted $BiFeO_3$ Epitaxial Thin Films at Morphotropic Phase Boundaries. *Appl. Phys. Lett.* **2010**, *97*, 212905.

(21) Lee, J.-H.; Oak, M.-A.; Choi, H. J.; Son, J. Y.; Jang, H. M. Rhombohedral−orthorhombic Morphotropic Phase Boundary in $BiFeO_3$-Based Multiferroics: First-Principles Prediction. *J. Mater. Chem.* **2012**, *22*, 1667−1672.

(22) González-Vázquez, O. E.; Wojdeł, J. C.; Diéguez, O.; Añiguez, J. First-Principles Investigation of the Structural Phases and Enhanced Response Properties of the $BiFeO_3$-$LaFeO_3$ Multiferroic Solid Solution. *Phys. Rev. B: Condens. Matter Mater. Phys.* **2012**, *85*, 064119.

(23) Karpinsky, D. V.; Troyanchuk, I. O.; Tovar, M.; Sikolenko, V.; Efimov, V.; Kholkin, A. L. Evolution of Crystal Structure and Ferroic Properties of La-Doped $BiFeO_3$ Ceramics near the Rhombohedral-Orthorhombic Phase Boundary. *J. Alloys Compd.* **2013**, *555*, 101−107.

(24) Troyanchuk, I. O.; Karpinsky, D. V.; Bushinsky, M. V.; Khomchenko, V. A.; Kakazei, G. N.; Araujo, J. P.; Tovar, M.; Sikolenko, V.; Efimov, V.; Kholkin, A. L. Isothermal Structural Transitions, Magnetization and Large Piezoelectric Response in $Bi_{1-x}La_xFeO_3$ Perovskites. *Phys. Rev. B: Condens. Matter Mater. Phys.* **2011**, *83*, 054109.

(25) Chen, D.; Nelson, C. T.; Zhu, X.; Serrao, C. R.; Clarkson, J. D.; Wang, Z.; Gao, Y.; Hsu, S.-L.; Dedon, L. R.; Chen, Z.; et al. A Strain-Driven Antiferroelectric-to-Ferroelectric Phase Transition in La-Doped $BiFeO_3$ Thin Films on Si. *Nano Lett.* **2017**, *17*, 5823−5829.

(26) Zalesskii, A. V.; Frolov, A. A.; Khimich, T. A.; Bush, A. A. Composition-Induced Transition of Spin-Modulated Structure into a Uniform Antiferromagnetic State in a $Bi_{1-x}La_xFeO_3$ System Studied Using ^{57}Fe NMR. *Phys. Solid State* **2003**, *45*, 141−145.

(27) Bielecki, J.; Svedlindh, P.; Tibebu, D. T.; Cai, S.; Eriksson, S.-G.; Börjesson, L.; Knee, C. S. Structural and Magnetic Properties of Isovalently Substituted Multiferroic $BiFeO_3$: Insights from Raman Spectroscopy. *Phys. Rev. B: Condens. Matter Mater. Phys.* **2012**, *86*, 184422.

(28) Chen, J.; Yu, R.; Li, H.; Sun, C.; Zhang, T.; Chen, H.; Xing, X. Structure and Shape Evolution of $Bi_{1-x}La_xFeO_3$ Perovskite Microcrystals by Molten Salt Synthesis. *Eur. J. Inorg. Chem.* **2008**, 3655−3660.

(29) Troyanchuk, I. O.; Bushinsky, M. V.; Karpinskii, D. V.; Mantytskaya, O. S.; Fedotova, V. V.; Prokhnenko, O. I. Structural Phase Transitions in the $Bi_{1-x}La_X$ FeO_3 System. *JETP Lett.* **2008**, *87*, 641−644.

(30) Troyanchuk, I. O.; Bushinsky, M. V.; Karpinsky, D. V.; Mantytskaya, O. S.; Fedotova, V. V.; Prochnenko, O. I. Structural Transformations and Magnetic Properties of Bi1-xLnxFeO3 (Ln = La, Nd, Eu). *Phys. Status Solidi B* **2009**, *246*, 1901−1907.

(31) Karpinsky, D. V.; Troyanchuk, I. O.; Mantytskaya, O. S.; Khomchenko, V. A.; Kholkin, A. L. Structural Stability and Magnetic

DOI: 10.1021/acsami.8b02597
ACS Appl. Mater. Interfaces 2018, 10, 14914−14921

Properties of $Bi1_{-x}La(Pr)_xFeO_3$ Solid Solutions. *Solid State Commun.* **2011**, *151*, 1686−1689.
(32) Karpinsky, D. V.; Troyanchuk, I. O.; Mantytskaja, O. S.; Chobot, G. M.; Sikolenko, V. V.; Efimov, V.; Tovar, M. Magnetic and Piezoelectric Properties of the $Bi_{1-X}La_XFeO_3$ System near the Transition from the Polar to Antipolar Phase. *Phys. Solid State* **2014**, *56*, 701−706.
(33) Yin, L. H.; Yang, J.; Zhao, B. C.; Liu, Y.; Tan, S. G.; Tang, X. W.; Dai, J. M.; Song, W. H.; Sun, Y. P. Large Remnant Polarization and Magnetic Field Induced Destruction of Cycloidal Spin Structure in $Bi_{1-x}La_xFeO_3$ ($0 \leq X \leq 0.2$). *J. Appl. Phys.* **2013**, *113*, 214104.
(34) Zeches, R. J.; Rossell, M. D.; Zhang, J. X.; Hatt, A. J.; He, Q.; Yang, C.-H.; Kumar, A.; Wang, C. H.; Melville, A.; Adamo, C.; et al. A Strain-Driven Morphotropic Phase Boundary in $BiFeO_3$. *Science* **2009**, *326*, 977−980.
(35) Carvalho, T. T.; Fernandes, J. R. A.; De La Cruz, J. P.; Vidal, J. V.; Sobolev, N. A.; Figueiras, F.; Das, S.; Amaral, V. S.; Almeida, A.; Moreira, J. A.; et al. Room Temperature Structure and Multiferroic Properties in $Bi_{0.7}La_{0.3}FeO_3$ Ceramics. *J. Alloys Compd.* **2013**, *554*, 97−103.
(36) Perejón, A.; Sánchez-Jiménez, P. E.; Pérez-Maqueda, L. A.; Criado, J. M.; de Paz, J. R.; Sáez-Puche, R.; Masó, N.; West, A. R. Single Phase, Electrically Insulating, Multiferroic La-Substituted BiFeO3 Prepared by Mechanosynthesis. *J. Mater. Chem. C* **2014**, *2*, 8398−8411.
(37) Chen, Z. H.; Damodaran, A. R.; Xu, R.; Lee, S.; Martin, L. W. Effect Of "symmetry Mismatch" on the Domain Structure of Rhombohedral $BiFeO_3$ Thin Films. *Appl. Phys. Lett.* **2014**, *104*, 182908.
(38) Troyanchuk, I. O.; Karpinsky, D. V.; Bushinsky, M. V.; Mantytskaya, O. S.; Tereshko, N. V.; Shut, V. N. Phase Transitions, Magnetic and Piezoelectric Properties of Rare-Earth-Substituted $BiFeO_3$ Ceramics. *J. Am. Ceram. Soc.* **2011**, *94*, 4502−4506.
(39) Zhang, T.; Li, W.; Hou, Y.; Yu, Y.; Cao, W.; Feng, Y.; Fei, W. Positive/negative Electrocaloric Effect Induced by Defect Dipoles in PZT Ferroelectric Bilayer Thin Films. *RSC Adv.* **2016**, *6*, 71934−71939.
(40) Ramazanoglu, M.; Ratcliff, W.; Yi, H. T.; Sirenko, A. A.; Cheong, S. W.; Kiryukhin, V. Giant Effect of Uniaxial Pressure on Magnetic Domain Populations in Multiferroic Bismuth Ferrite. *Phys. Rev. Lett.* **2011**, *107*, 067203.
(41) Sando, D.; Agbelele, A.; Rahmedov, D.; Liu, J.; Rovillain, P.; Toulouse, C.; Infante, I. C.; Pyatakov, A. P.; Fusil, S.; Jacquet, E.; et al. Crafting the Magnonic and Spintronic Response of $BiFeO_3$ Films by Epitaxial Strain. *Nat. Mater.* **2013**, *12*, 641−646.
(42) Artman, J. O.; Murphy, J. C.; Foner, S. Magnetic Anisotropy in Antiferromagnetic Corundum-Type Sesquioxides. *Phys. Rev.* **1965**, *138*, A912−A917.
(43) Karthik, J.; Damodaran, A. R.; Martin, L. W. Epitaxial Ferroelectric Heterostructures Fabricated by Selective Area Epitaxy of $SrRuO_3$ Using an MgO Mask. *Adv. Mater.* **2012**, *24*, 1610−1615.
(44) Li, J.; Jin, E.; Son, H.; Tan, A.; Cao, W. N.; Hwang, C.; Qiu, Z. Q. Design of a Vector Magnet for the Measurements of Anisotropic Magnetoresistance and Rotational Magneto-Optic Kerr Effect. *Rev. Sci. Instrum.* **2012**, *83*, 33906.

DOI: 10.1021/acsami.8b02597
ACS Appl. Mater. Interfaces 2018, 10, 14914−14921